Available online at www.sciencedirect.com

SciVerse ScienceDirect

Geochimica et Cosmochimica Acta 89 (2012) 46–61

Geochimica et Cosmochimica Acta

www.elsevier.com/locate/gca

Experimental determination of iron isotope fractionations among Fe^{2+}_{aq}–FeS_{aq}–Mackinawite at low temperatures: Implications for the rock record

Lingling Wu [a,b,*], Greg Druschel [c,d], Alyssa Findlay [c], Brian L. Beard [a,b], Clark M. Johnson [a,b]

[a] Department of Geoscience, University of Wisconsin-Madison, 1215 West Dayton Street, Madison, WI 53706, United States
[b] NASA Astrobiology Institute, University of Wisconsin-Madison, Madison, WI 53706, United States
[c] Department of Geology, University of Vermont, 180 Colchester Ave, Burlington, VT 05405, United States
[d] Department of Earth Sciences, Indiana University-Purdue University, Indianapolis, 723 W. Michigan St., Indianapolis, IN 46202, United States

Received 10 November 2011; accepted in revised form 23 April 2012; available online 30 April 2012

Abstract

The Fe isotope fractionation factors among aqueous ferrous iron (Fe^{2+}_{aq}), aqueous FeS clusters (FeS_{aq}), and nanoparticulate mackinawite under neutral and mildly acidic and alkaline pH conditions have been determined using the three-isotope method. Combined voltammetric analysis and geochemical modeling were used to determine the Fe speciation in the experimental systems. The equilibrium $^{56}Fe/^{54}Fe$ fractionation factor at 20 °C and pH 7 has been determined to be -0.32 ± 0.29 $(2\sigma)‰$ between Fe^{2+}_{aq} (minor FeS_{aq} also present in the experiment) and mackinawite. This fractionation factor was essentially constant when pH was changed to 6 or 8. When equal molarity of HS^- and Fe^{2+}_{aq} were added to the system, however, the isotopic fractionation at pH 7 changed to -0.64 ± 0.36 $(2\sigma)‰$, correlating with a significant increase in the proportion of $FeHS^+$ and FeS_{aq}. These results highlight a more important role of aqueous Fe–S speciation in the equilibrium Fe isotope fractionation factor than recognized in previous studies. The isotopic fractionation remained constant when temperature was increased from 20 °C to 35 °C for fractionation factors between Fe^{2+}_{aq}, and mackinawite and between dominantly $FeHS^+$ and mackinawite. Synthesis experiments similar to those of Butler et al. (2005) and Guilbaud et al. (2010) at pH 4 show consistent results: over time, the aqueous Fe–mackinawite fractionation decreases but even after 38 days of aging the fractionation factor is far from the equilibrium value inferred using the three-isotope method. In contrast, at near-neutral pH the fractionation factor for the synthesis experiment reached the equilibrium value in 38 days. These differences are best explained by noting that at low pH the FeS mackinawite particles coarsen more rapidly via particle aggregation, which limits isotopic exchange, whereas at higher pH mackinawite aggregation is limited, and Fe isotope exchange occurs more rapidly, converging on the equilibrium value. These results suggest that mackinawite formed in natural environments at near-neutral or alkaline pH are unlikely to retain kinetic isotope fractionations, but are more likely to reflect equilibrium isotope compositions. This in turn has important implications for interpreting iron isotope compositions of Fe sulfides in natural systems.
© 2012 Elsevier Ltd. All rights reserved.

* Corresponding author. Current address: Department of Earth and Environmental Sciences, University of Waterloo, Waterloo, ON, Canada N2L 3G1. Tel.: +1 5198884567x38674.
E-mail address: lingling.wu@uwaterloo.ca (L. Wu).

0016-7037/$ - see front matter © 2012 Elsevier Ltd. All rights reserved.
http://dx.doi.org/10.1016/j.gca.2012.04.047

1. INTRODUCTION

Sulfide minerals define the largest range in Fe isotope compositions measured on Earth. The δ^{56}Fe values of Archean sedimentary pyrite and pyrite-bearing shales range from −3.7‰ to +2.1‰ (Rouxel et al., 2005; Yamaguchi et al., 2005; Archer and Vance 2006; Dauphas et al., 2007; Whitehouse and Fedo 2007; Hofmann et al., 2009; Nishizawa et al., 2010). The origin of the large number of negative δ^{56}Fe values, which are striking relative to the near-zero δ^{56}Fe values of bulk continental and oceanic crust, remains contentious (e.g., Archer and Vance 2006; Rouxel et al., 2006; Yamaguchi and Ohmoto, 2006). Rouxel et al. (2005) interpret low δ^{56}Fe values to reflect the Fe isotope compositions of the Archean oceans under an anoxic atmosphere, whereas Archer and Vance (2006) interpret low-δ^{56}Fe sedimentary pyrite to indicate coupled bacterial sulfate- and Fe^{3+}-reduction, based on δ^{34}S–δ^{56}Fe correlations. In contrast to previous interpretations that pyrite is a passive recorder of the aqueous Fe^{2+} (Fe^{2+}_{aq}) pool and that the wide range in δ^{56}Fe values reflects Fe redox changes, Guilbaud et al. (2011a) argue that the negative δ^{56}Fe excursion in sulfides from Neoarchean and Paleoproterozoic rocks may reflect partial Fe^{2+}_{aq} utilization during abiotic pyrite formation, based on a combined kinetic isotope fractionation between Fe^{2+}_{aq} and mackinawite, and between mackinawite and pyrite. This interpretation, however, has been debated (Czaja et al., 2012; Guilbaud et al., 2012). Low-δ^{56}Fe pyrite is so far absent in most of the Proterozoic rock record, where values become generally positive, up to +2.1‰ (Rouxel et al., 2005; Nishizawa et al., 2010). Any solution to this debate must explain the temporal changes in δ^{56}Fe values for pyrite, and reconcile the fact that theory predicts pyrite should have the highest δ^{56}Fe values of any of the common minerals found in surface environments (Polyakov et al., 2007).

Mackinawite is an important precursor phase to pyrite in marine sedimentary environments (e.g., Schoonen and Barnes, 1991; Wei and Osseo-Asare, 1996; Rickard, 1997; Benning et al., 2000; Butler and Rickard 2000; Schoonen 2004). It has been suggested that several different pathways may be important in pyrite formation in natural low-temperature systems. The H_2S pathway was first recognized by Taylor et al. (1979) and involves H^+ as the electron acceptor (e.g., Rickard, 1997; Rickard and Luther, 1997). In contrast, the S^0 addition and polysulfide pathways involve S as the electron acceptor (e.g., Berner, 1970; Rickard, 1975; Luther, 1991). These pathways all involve precursor FeS phases, which appear to be essential to pyrite formation in low-temperature (<100 °C) environments (e.g., Morse et al., 1987; Rickard et al., 1995; Schoonen, 2004).

Formation of aqueous metal-sulfide clusters, which we define as FeS_{aq} in the case of Fe (equivalent to Fe_XS_Y where X and Y are unknown but less that 150; Luther and Rickard, 2005), is an important pathway leading to sulfide mineral formation, including Fe, Cu, and Zn sulfides (e.g., Thompson and Helz, 1994; Theberge and Luther, 1997; Davison et al., 1999; Luther et al., 1999; Butler and Rickard, 2000; Labrenz et al., 2000; Luther et al., 2002; Wolthers et al., 2003; Druschel et al., 2004; Luther and Rickard, 2005). Rickard et al. (2006) determined the equilibrium of mackinawite with a monomer of the FeS_{aq} cluster ($FeS_{mack} = FeS^0$) to have a log K of −5.7, and the equilibrium of mackinawite and Fe^{2+} and H_2S to have a log K of 3.5:

$$FeS_{mack} \leftrightarrow FeS_{aq} \log K = -5.7$$

$$FeS_{mack} + 2H^+ \leftrightarrow Fe^{2+} + H_2S \log K = 3.5$$

The large bonding changes that occur between hexaquo Fe^{2+} ($Fe(H_2O)_6^{2+}$), where Fe^{2+} is in octahedral coordination (e.g., Cotton et al., 1993), and FeS_{aq}, where Fe^{2+} is in tetrahedral coordination (Theberge and Luther, 1997; Luther and Rickard, 2005), may be accompanied by significant Fe isotope fractionations, drawing upon analogies with other transition metal species (e.g., Schauble, 2004). Indeed, it is possible that the isotopic fractionation between Fe^{2+}_{aq} and FeS_{aq} could be the major factor in which the Fe isotope compositions of sulfide minerals are determined. In diagenetic systems that eventually form sulfide minerals, the following reaction represents an important pathway in marine systems when Fe^{2+}_{aq} is present (e.g., Liu and Millero, 2002; Butler, 2005):

$$Fe^{2+}_{aq} + H_2S \text{ or } HS^- \rightarrow FeS_{aq} \rightarrow FeS_{mack}$$

Butler et al. (2005) determined an initial $^{56}Fe/^{54}Fe$ fractionation factor of ∼+0.9‰ between Fe^{2+}_{aq} and mackinawite, which changed to ∼+0.3‰ over time, in Fe^{2+}-dominated pH 4 solutions, which they attribute to a kinetic fractionation that is independent of temperature. Butler et al. (2005) inferred that the equilibrium Fe^{2+}_{aq}–mackinawite fractionation was <+0.3‰. Guilbaud et al. (2010) extended the previous experiments of Butler et al. to longer time periods and found that the kinetic fractionation between Fe^{2+}_{aq} and mackinawite changed from an initial fractionation of ∼+1.2‰ to ∼+0.3‰ after 30 days, and they inferred that isotopic exchange was kinetically restricted at low temperatures. In a subsequent study, using the three-isotope method (e.g., Matsuhisa et al., 1978; Beard et al., 2010), Guilbaud et al. (2011b) determined the equilibrium fractionation factor between Fe^{2+}_{aq} and mackinawite to be -0.33 ± 0.12‰ at 25 °C and pH 4. That the results of Butler et al. (2005) and Guilbaud et al. (2010) were far from equilibrium demonstrates that the three-isotope method provides a more rigorous assessment of isotopic exchange kinetics and extent of isotopic exchange than use of natural isotopic compositions. Moreover, the three-isotope method allows extrapolation of systems that underwent partial isotopic exchange to 100% exchange to infer equilibrium fractionation factors.

In this contribution, we apply the three-isotope method to the system Fe^{2+}_{aq}–FeS_{aq}–mackinawite, extending the results of Butler et al. (2005) and Guilbaud et al. (2011b) in several key areas. First, experiments in the current study were run at pH 4, 6, 7, and 8, a range of pH significantly higher than the pH 4 experiments of Butler et al. (2005) and Guilbaud et al. (2011b). The higher pH is more appropriate to marine environments, particularly in systems where bacterial sulfate reduction occurs, which produces alkalinity. The effects of pH on particle coarsening

(coarsening here defined as a combination of particle ripening and aggregation) were also investigated under these experimental conditions to test the hypothesis by Guilbaud et al. (2010) that the rate of particle coarsening affects rates of isotopic exchange. Second, we explore the isotopic fractionation between hexaquo Fe^{2+} (represented as Fe^{2+}_{aq}) and FeS_{aq} through varying sulfide contents and hence aqueous speciation, where speciation was monitored using voltammetry. Guilbaud et al. (2011b) proposed that the major fractionation between aqueous Fe and mackinawite occurs between hexaquo Fe^{2+} and FeS_{aq} and predicted that the Fe isotope fractionation between FeS_{aq} and mackinawite would be insignificant, and the variations we explored in aqueous Fe speciation test this prediction. Third, we used dialysis membranes to attain complete separation of aqueous Fe and nanoparticulate mackinawite. Ohfuji and Rickard (2006) noted that the first condensed phases of mackinawite are tabular particles 2–6 nm thick by 3–11 nm long, and even with significant particle aggregation, some of these particles may pass through laboratory filters. Effective separation of aqueous Fe and nanoparticles of mackinawite is especially important when using enriched isotope tracers because cross-contamination would produce larger apparent amounts of isotopic exchange. We conclude this contribution by comparing the experimental results to Fe isotope variations in natural environments where Fe–S cycling occurs.

2. MATERIALS AND METHODS

2.1. Experimental designs

Experiments investigating isotopic exchange kinetics and equilibrium fractionations between mackinawite and Fe^{2+}_{aq} or FeS_{aq} (Experiments 3-2 to 3-6, Table 1) were carried out using dialysis membranes at the University of Vermont. Initial experiments (Experimental sets 1 and 2, Supplementary Table S1) determined the most efficient membrane size, solution ionic strength, and proportions of Fe species required to ensure fast diffusion of Fe^{2+}_{aq}, FeS_{aq}, H_2S, and HS^- across the membrane, yet maintain complete retention of nanoparticulate mackinawite inside the membrane. Isotopic exchange experiments using dialysis membranes (Experiments 3-2 to 3-6) used a solution internal to the membrane container that contained a suspension of ^{57}Fe-enriched mackinawite (FeS_{mack}) and a solution external to the membrane that contained isotopically "normal" Fe^{2+}_{aq}, with or without additional sulfide. In both the internal and external solutions a 10 mM PIPES buffer was used to maintain pH, and 0.1 M KBr was added to provide ionic strength to facilitate isotopic exchange, as demonstrated by the dialysis membrane tests of Experiment sets 1 and 2 (see details in Supplementary Information). The ^{57}Fe-enriched mackinawite was synthesized by mixing equimolar quantities of ^{57}Fe-enriched Fe^{2+}_{aq} and sulfide. Stock solutions of Fe^{3+} were first prepared by dissolving a mixture of ^{57}Fe-enriched oxide (Oak Ridge National Lab) and isotopically "normal" Fe_2O_3 in hot HCl for several days. Fe^{2+}_{aq} solutions were produced by addition of excess sodium sulfite at pH <2 (reducing Fe^{3+}_{aq} to Fe^{2+}_{aq}), followed by titration of NaOH to desired pH values. Sulfide solutions were prepared fresh for each experiment from sodium sulfide nonahydrate salts washed under O_2-free 18 MΩ water, dried, weighed, and dissolved in O_2-free 18 MΩ water. All preparations and experiments were done inside an anaerobic chamber (Coy Products). The mackinawite slurry was stirred to maintain as homogeneous a suspension as possible before aliquots of the slurry were added to individual experimental reactors. 10 ml of the internal mackinawite slurry was added to a float-a-lyzer, sealed with a screw cap, and suspended in 100 ml of the external solution in a 120 ml glass tube that was then sealed with a rubber septum. Separate reactors were prepared to allow sampling at different time points of each experiment; as such, slightly different molar proportions of isotopically "enriched" and "normal" Fe were added, but this was accounted for, as described in Section 2.4 below.

Experimental set 3-1 (Table 1) was done at the University of Wisconsin-Madison without a dialysis membrane, following the experimental configuration used by Guilbaud et al. (2011b), but at pH 7, in contrast to the pH 4 conditions used by Guilbaud et al. (2011b). Two subsets of isotopic exchange experiments were conducted without a dialysis membrane: (1) isotopically "normal" Fe^{2+}_{aq} + ^{57}Fe-enriched mackinawite (duplicate Experiments 3-1a and 3-1b), and (2) a reversal, using ^{57}Fe-enriched Fe^{2+}_{aq} + "normal" mackinawite (duplicate Experiments 3-1c and 3-1d). Experiments were carried out in separate 10 ml serum glass bottles with 10 ml of a solution that contained 10 mM anoxic PIPES buffer and 0.1 M KBr, and a final pH adjusted to 7. A stock solution of ferrous Fe that had a "normal" isotopic composition was prepared by dissolving $FeCl_2{\cdot}4H_2O$ in 0.5 M HCl in an anaerobic chamber. A ^{57}Fe-enriched ferrous stock solution was prepared by first dissolving pure ^{57}Fe metal (Chemgas) in HCl and then mixing with isotopically "normal" ferrous solution to attain a δ^{57}Fe value of ~100‰. This level of enrichment is sufficient to provide precise estimates of the extent of isotopic exchange. A stock solution of mackinawite was prepared by mixing equal molar quantities of either "normal" or ^{57}Fe-enriched Fe^{2+}_{aq} and sulfide, followed by filtration and resuspending in water. The experiments were initiated by addition of $FeCl_2$ and mackinawite from their stock solutions. Sampling was done by filtering mackinawite particles with a 0.22 μm size filter paper inside the anaerobic chamber at different time points, which is identical to the approach used by Guilbaud et al. (2011b).

A final set of experiments (Experiment set 4, Table 1) was based on synthesis experiments conducted by Butler et al. (2005), where FeS_{mack} was precipitated by mixing an Fe^{2+}_{aq} solution (prepared from Mohr's salt, $(NH_4)_2Fe(SO_4)_2{\cdot}6H_2O$) and sulfide solution at a 10:1 Fe:S ratio. The original experiments of Butler et al. (2005) were carried out at pH 4, using 50 mM Fe^{2+}_{aq} and 5 mM HS^- over one week. Follow-up experiments were run for one month at pH 4 by Guilbaud et al. (2010). We expanded the synthesis experiments to 6 weeks of reaction time and added additional experiments at pH 7 and 8. For these experiments, the suspension was filtered through a 0.22 μm filter to separate

Table 1
Comparison of experimental conditions in this study and previous work investigating Fe isotope fractionation between Fe^{2+} and mackinawite.

Experiments	Isotopic tracer	Dialysis membrane	pH	Duration (days)	Temp (°C)	Fe (μM)	Na_2S (μM)	References
Isotopic exchange experiments								
	^{56}Fe-enriched mackinawite	No	4	32	2	50,000	0	Guilbaud et al. (2011)
	^{56}Fe-enriched mackinawite	No	4	120	25	50,000	0	Guilbaud et al. (2011)
3-1a and 3-1b	^{57}Fe-enriched mackinawite	No	7	23	20	100	0	This study
3-1c and 3-1d	^{57}Fe-enriched Fe^{2+}_{aq}	No	7	23	20	100	0	This study
3-2	^{57}Fe-enriched mackinawite	Yes	7	23	20	50	50	This study
3-3	^{57}Fe-enriched mackinawite	Yes	7	24	35	100	0	This study
3-4	^{57}Fe-enriched mackinawite	Yes	7	12	35	50	50	This study
3-5	^{57}Fe-enriched mackinawite	Yes	8	27	20	100	0	This study
3-6	^{57}Fe-enriched mackinawite	Yes	6	24	20	100	0	This study
Synthesis experiments								
	No	No	4	7	20	50,000	5000	Butler et al. (2005)
	No	No	4	0	2	50,000	5000	Butler et al. (2005)
	No	No	4	0	10	50,000	5000	Butler et al. (2005)
	No	No	4	0	40	50,000	5000	Butler et al. (2005)
	No	No	4	27	25	50,000	5000	Guilbaud et al. (2010)
	No	No	4	30	2	50,000	5000	Guilbaud et al. (2010)
4-1 and 4-2b and 4-1b F1	No	No	7	38	20	50,000	5000	This study
4-1b F2[a]	No	No	7	23	20	50,000	5000	This study
4-1c and 4-2	No	No	4	38	20	50,000	5000	This study
4-3	No	No	8	23	20	50,000	5000	This study
4-4	No	No	7	19	20	5000	500	This study
4-5	No	No	8	19	20	5000	500	This study

[a] All samples in this study were filtered through a 0.22 μm filter except Experiment 4-1b F2 where a 0.025 μm filter was used. Separate reactors were prepared for each time point.

the mackinawite from the solution. A replicate experimental set was also done by filtering the slurry through a 0.025 μm filter to separate the mackinawite from solution.

2.2. Fe phase separation and wet chemical analysis

Solutions from each of the experiments were analyzed to determine the iron and sulfur speciation by a combination of *in situ* solid state Au-amalgam voltammetry, dropping mercury electrode (DME) polarography, colorimetry, inductively coupled plasma optical emission spectroscopy (ICP-OES), and pH measurements. *In situ* voltammetry was done by passing a set of connector wires through a sealed access plug on the anaerobic chamber, allowing electrodes to be used inside the chamber but controlled outside the chamber by an Analytical Instrument Systems DLK-60 potentiostat and computer controller (see details in Supplementary Information). Solid samples of Fe–S materials were collected by either filtration (for X-ray Diffraction analysis) or by subsampling the experiment slurry (for Raman and dynamic laser particle scattering analysis) inside the anaerobic chamber and analyzed immediately (see details in Supplementary Information).

2.3. Fe isotope measurement and nomenclature

Prior to isotopic analysis, all samples were purified using anion-exchange chromatography, following the methods of Beard et al. (2003). Iron isotope analyses were performed on separated aqueous Fe (of mixed Fe^{2+}_{aq} and FeS_{aq} species) and mackinawite phases using a multi-collector, inductively coupled plasma mass spectrometer (MC-ICP-MS, UW-Madison, WI) following established protocols (Beard et al., 2010). A fast-washout spray chamber and a decreased potential difference between extraction and skimmer cones were employed to avoid memory effects.

Iron isotope compositions are described using standard δ notation, in units of per mil (‰):

$$\delta^{56}Fe = \left[\frac{^{56}Fe/^{54}Fe_{sample}}{^{56}Fe/^{54}Fe_{std}} - 1\right] \times 10^3 \quad (1)$$

and

$$\delta^{57/56}Fe = \left[\frac{^{57}Fe/^{56}Fe_{sample}}{^{57}Fe/^{56}Fe_{std}} - 1\right] \times 10^3 \quad (2)$$

where the $^{56}Fe/^{54}Fe_{std}$ and $^{57}Fe/^{56}Fe_{std}$ are the average of igneous rocks (Beard et al., 2003). The isotopic fractionation between two phases A and B is defined as

$$\alpha^{56}_{A\text{-}B} = \frac{^{56}Fe/^{54}Fe_A}{^{56}Fe/^{54}Fe_B} \quad (3)$$

following standard practice. To a very good approximation, $\alpha^{56}_{A\text{-}B}$ may be related to differences in the $\delta^{56}Fe$ values through the relation:

$$\Delta^{56}Fe_{A\text{-}B} = \delta^{56}Fe_A - \delta^{56}Fe_B \approx 10^3 \ln\alpha^{56}_{A\text{-}B} \quad (4)$$

The extent of isotopic exchange is best monitored using the $^{57}Fe/^{56}Fe$ ratios because an enriched-^{57}Fe tracer was used.

The measured Fe isotope composition of the IRMM-014 Fe isotope standard was $\delta^{56}Fe = -0.10 \pm 0.03‰$ and $\delta^{57/56}Fe = -0.03 \pm 0.06‰$ (average and 1-standard deviation of 22 analyses), on the igneous rock scale. Based on replicate analyses of standards and samples processed through the entire analytical procedure, both the $\delta^{56}Fe$ and $\delta^{57/56}Fe$ values are accurate and precise to 0.05‰ (1σ, $n = 85$) using the fast-washout spray chamber.

2.4. Calculation of fraction of isotopic exchange (F)

The extent of isotopic exchange (F) towards 100% exchange is calculated by:

$$F = \frac{\delta - \delta_i}{\delta_e - \delta_i} \quad (5)$$

where δ is the isotope composition at any time, δ_i is the isotope composition of the starting material, and δ_e is the equilibrium isotope composition calculated from the mass balance of each reactor. Although δ_e is difficult to estimate for exchange experiments involving "normal" isotopic compositions, it is accurately calculated for enriched isotope tracer experiments, such as those used here and by Guilbaud et al. (2011b). The mass balance of the system was constrained within 13% error for all the exchange experiments (Supplementary Tables S1 and S2). The isotopic composition of the starting mackinawite (Supplementary Table S2) was directly measured for Experiment 3-1 series where no dialysis membrane was used. For experiments where a dialysis membrane was used (3-2 to 3-6), the starting composition of mackinawite was calculated using the average mass balance of different reactors for each experiment and the isotopic composition of the aqueous component, which is assumed to be constant in all the experiments and equal to that used in the preliminary experiments (Experiment sets 1 and 2, Supplementary Table S1). This assumption is supported by the almost identical isotopic compositions for the aqueous component within analytical errors in the preliminary experiments (Supplementary Table S1). The large errors in $\delta^{57/56}Fe$ values of the starting mackinawite reflect variations of mass balance in the system and the difficulty in homogenizing the mackinawite slurry when added to individual reactors. Importantly, calculation of F using either the aqueous component or mackinawite agreed within 10% except for a few early time points (see Supplementary Table S2). It is important to highlight that we obtained good agreement in the calculation of F using either solid or aqueous components, which provides an independent check on mass balance, as well as any issues of solid-sample separation. The coincidence of these results indicates that the uncertainty in the $\delta^{57/56}Fe$ values for the initial mackinawite impart only a small uncertainty in the calculated amount of isotopic exchange.

2.5. Optimal experimental conditions for use of dialysis membranes for separation of nanoparticles

Use of dialysis membranes for separation of nanoparticles is a promising approach for studies of fluid–mineral interactions, suitable for study of solubility or exchange properties where physical separation of solids from liquids is needed, but difficult due to very small particle size. Considering the small particle size of mackinawite, our initial concern was that filtration methods used in previous studies (Butler et al., 2005; Guilbaud et al., 2010; Guilbaud et al., 2011b) may not have been sufficient for separating the solid from the aqueous phase. In order to evaluate the possibility that incomplete solid–liquid separation may cause artificially high fractions of exchange (F) to be calculated, and thus a smaller estimated equilibrium fractionation factor, we conducted experiments using dialysis membranes of different porosity to fully separate aqueous and solid components. This new approach, however, poses significant technical challenges, in terms of attaining adequate transport of soluble species across the membrane while still separating nanoparticulate mackinawite from aqueous Fe. Enriched ^{57}Fe-tracer experiments were done in the absence of solid materials, and these showed that isotopic exchange between aqueous Fe^{2+} inside and outside of the membrane was much faster in 0.1 M KBr solution than that in 0.1 M KCl solution (56% exchange after 17 h versus 5% exchange after 26 h, see Experiments 1-6 and 1-6b in Supplementary Table S1). Similarly fast rates were observed when both Fe^{2+} and HS^- were present, under conditions where $FeHS^+$ was the dominant form of aqueous Fe (see Section 3.1. for speciation information), in 0.1 M KBr solution (57% exchange after 24 h, Experiment 1-8). Increasing the membrane size from 5 K Dalton to 15 K Dalton increased the exchange rate for Fe^{2+} across the membrane to 32% after 46 h in 0.1 M KCl solution (Experiment 2-1b), and close to 100% exchange occurred after 48 h in 0.1 M KBr solution (Experiments 2-2c and 2-10). Complete exchange was also achieved for both Fe^{2+} and HS^- across the membrane after 48 h when using a 15 K Dalton membrane and 0.1 M KBr solution (Experiment 2-3c).

Membrane exchange experiments were also done with mackinawite inside the membrane to reproduce experimental conditions in the mackinawite exchange experiments. These experiments were not designed to measure equilibrium fractionation between aqueous Fe and mackinawite but to determine isotopic transport rates of aqueous species across the membranes in the presence of mackinawite. The major proportion of total iron was ^{57}Fe-enriched mackinawite in these systems compared with approximately equal mass proportion of aqueous Fe and mackinawite in later exchange experiments. This set of experiments also varied the ratio of the volume inside the membrane to the volume outside the membrane, using ratios of 1:10 and 1:20. In addition to use of a 15 K Dalton membrane, 100 K Dalton membranes were tested. Using a 15 K Dalton membrane and 0.1 M KBr solution produced 67% exchange after 48 h when the volume ratio of the dialysis membrane versus the containing glass vessel was 1:10 (Experiment 2-4c), and 81% exchange after 48 h when the volume ratio was 1:20 (Experiment 2-5c). Increasing the membrane size to 100 K Dalton did not significantly increase the exchange rate between mackinawite and aqueous Fe (Experiment 2-5), and this suggests that effective aqueous species size was much smaller than 100 K Dalton. In summary, use of a 15 K Dalton membrane and 0.1 M KBr solution, which we speculate

minimizes charge buildup on the membrane surface, seemed to maximize the transport of aqueous Fe^{2+} and FeS_{aq} across the membrane. Aqueous Fe and S species are inferred to diffuse more slowly through the 5 K Dalton membrane pores, and faster through the 15 K Dalton membrane pores. Although the exchange across the membrane required 48 h to reach 100% isotopic equilibrium, over the timescales and exchange extent of the experiments by Guilbaud et al. (2011b), as well as our experiments discussed below, trans-membrane exchange rates are several orders-of-magnitude faster than exchange between nanoparticulate mackinawite and aqueous Fe.

3. RESULTS

3.1. Aqueous Fe and S speciation

Two experimental sets (set 3 and 4) utilized different concentration ranges of iron and sulfide, as well as different Fe:S ratios and pH values, to probe possible control of iron and sulfur speciation on the Fe isotope fractionations. These changes also produced differences in particle aggregation rates, which in turn could affect isotopic exchange rates. All experiments maintained equivalent amounts of Fe^{2+}_{aq} and FeS_{aq} over the experimental duration, although it is possible that there were changes in the specific molecular size and structure of FeS_{aq}. Such changes potentially would have affected transport across the membrane or isotopic fractionation if they imparted significant changes in Fe bonding. It is not possible, however, to quantify such changes.

Experiment set 3 (Supplementary Table S2) investigated lower concentration ranges of iron (100 μM Fe^{2+} only). A subset of these experiments used 50 μM Fe^{2+} and 50 μM HS^- to form a metastable FeS_{aq} solution. Aqueous speciation was monitored using voltammetry (see Fig. 1 for a representative analysis), and these measurements indicated that the predominant species in the Fe-only experiments (3-1, 3-3, 3-5, 3-6) was $Fe(H_2O)^{2+}_6$. For experiments with iron and sulfide added, the proportion of FeS_{aq} species increased significantly (Experiments 3-2, 3-4). The FeS_{aq} cluster has a more positive potential than Fe^{2+}_{aq}, and the shift in the cathodic voltammogram obtained using 100 μM Fe^{2+}, relative to 50 μM Fe^{2+} and 50 μM HS^-, indicates a change in major iron speciation towards the aqueous FeS cluster (FeS_{aq}). It is important to note that we cannot quantify the exact amount of FeS_{aq} in these solutions by voltammetry, because there is no calibration of voltammetry based on the specific sizes of aqueous FeS clusters. The voltammetry results, however, demonstrate that we achieved significant differences in the proportions of $Fe(H_2O)^{2+}_6$ and FeS_{aq} over the range of our experimental conditions.

Experiment set 4 investigated conditions similar to those used by Butler et al. (2005), which is fundamentally a mackinawite synthesis experiment rather than an isotopic exchange experiment, although our experiments were run at pH 7 in addition to the pH 4 conditions used by Butler et al. (2005). Two mixtures of Fe and S were used, one at 50 mM Fe^{2+} and 5 mM HS^-, and one at 5 mM Fe^{2+} and 0.5 mM HS^- (Supplementary Table S3). Aqueous speciation determined by voltammetry indicates that the predominant iron species was $Fe(H_2O)^{2+}_6$ under these conditions. At pH 4 (as in Butler et al., 2005) there is no definable FeS_{aq} moiety, but in our experiments at pH 7 there is significant FeS_{aq} in solution. It is important to note that in none of these experiments was 'free' sulfide present. The voltammetric methods used for analysis have a detection limit for "free" sulfide in the nanomolar range (Glazer et al., 2006).

Thermodynamic modeling was done using Geochemist's Workbench program 6.0 and an adjusted minteq database with additional data for mackinawite and FeS_{aq} data from Benning et al. (2000) and Rickard et al. (2006), respectively. Three representative fluid compositions in equilibrium with mackinawite for the experiments conducted were speciated across the range of pH values tested (Fig. 2A–C). Modeling of solution compositions indicates that in the Fe-only (no added sulfide) experiments (3-1, 3-5, 3-6, see Fig. 2A), the predominant form of aqueous iron was $Fe(H_2O)^{2+}_6$, and FeS_{aq} was four orders-of-magnitude lower. For the

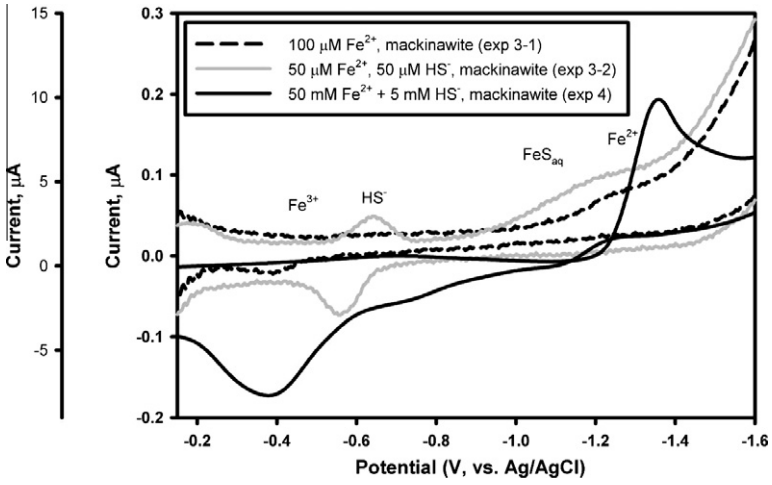

Fig. 1. Representative voltammograms for Experiment sets 3 and 4. Far left *y* axis is scale for Experiment set 4; note that the current spans a much larger range and the potential shifts more negatively for the Fe^{2+} peak with higher concentration of Fe^{2+} for Experiment set 4.

experiments with 50 μM Fe^{2+} and 50 μM HS^- (Experiment 3-2, see Fig. 2B) $FeHS^+$ becomes the dominant species with increasing pH, followed by an increasing proportion of FeS_{aq}. For Experiment set 4 (50 mM Fe^{2+} and 5 mM H_2S; Fig. 2C), the major aqueous species was $Fe(H_2O)_6^{2+}$ across all pH values. The molar proportion of different aqueous Fe species for Experiment 3-1 at pH 7 is 99.6% $Fe(H_2O)_6^{2+}$, 0.29% $FeOH^+$, 0.09% $FeHS^+$ and 0.01% FeS_{aq}. For Experiment 3-2, where equal molarity of HS^- and Fe^{2+} were used, the proportions were 63.2% $FeHS^+$, 28.2% $Fe(H_2O)_6^{2+}$, 8.52% FeS_{aq}, and 0.08 $FeOH^+$. $FeHS^+$ does not interact as a separate moiety at the electrode surface (Luther and Ferdelman, 1993; Luther et al., 1996), and voltammetric measurements of the Fe^{2+}_{aq}, H_2S, and HS^- present in these solutions were largely consistent with these calculations. FeS_{aq} is observed voltammetrically at pH lower than what the speciation calculations suggests, consistent with observations in other circumneutral pH environments (Theberge and Luther, 1997; Luther et al., 2003; Druschel et al., 2008). It is important to note that the presence of 0.1 M KBr in the solutions, which was added to increase transport across the dialysis membranes, does not significantly affect the Fe speciation in the experiments as inferred from our thermodynamic calculations.

3.2. Solid phase characterization

X-ray diffraction data were obtained on all precipitated Fe–S materials, and these data indicate that under all conditions the Fe–S solids that were produced were comprised of at least 90% mackinawite, with minor amounts of smythite (a slightly iron-deficient Fe–S mineral). Samples analyzed immediately after collection in the anaerobic chamber showed no detectable amounts of oxidized iron materials, and no degree of pyritization to form greigite or pyrite.

The size of the mackinawite particulates (here defined as either single crystals or aggregates of crystals; the dynamic light scattering techniques utilized do not distinguish between the two) was affected by changing pH and Fe:S ratios of the starting solutions. Particulate size changes (or coarsening, here defined as including both individual particle size and particle aggregate size changes) were fastest for lower pH and higher Fe:S ratio systems (Fig. 3). For Experiment set 3, the pH and Fe:S ratios employed would have experienced relatively slow particle coarsening. Conversely, under the experimental conditions of Experiment set 4, especially those at pH 4 that were intended to mimic conditions used by Butler et al. (2005), rapid particle coarsening occurred (Fig. 3).

This in turn indicates that the mackinawite particulates likely contained a rapidly coarsening non-exchanging core that hindered further isotopic exchange between aqueous Fe^{2+} and mackinawite over time (Guilbaud et al., 2010). As will be discussed below, the inhibited isotopic exchange was clearly demonstrated by slower exchange in synthesis experiments at pH 4 as compared with that at pH 7.

3.3. Equilibrium fractionation factors between aqueous Fe and mackinawite

The isotope exchange kinetics discussed in Section 2.5 indicate that the long-term extents of exchange for experiments that used dialysis membranes are likely to be accurate given the rapid exchange across the membranes. Moreover, the long-term extents of exchange in experiments that did not use dialysis membranes are also likely to be accurate, because coarsening allowed efficient solid–liquid separation even without a dialysis membrane, as discussed in Section 3.2. Therefore, the equilibrium Fe

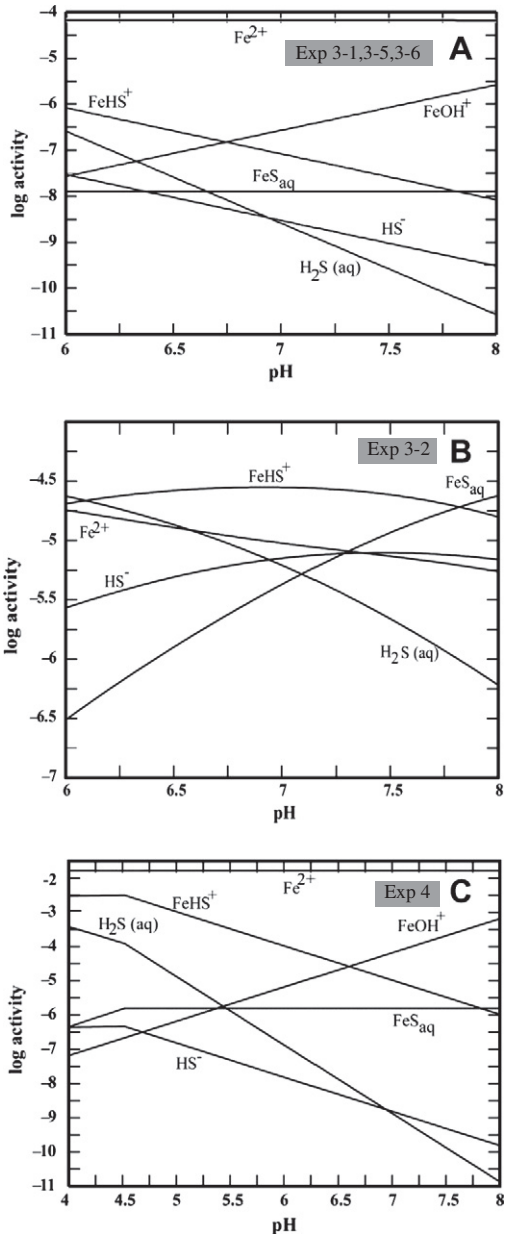

Fig. 2. Calculated speciation of iron and sulfur over the ranges of pH conditions for Experiment sets 3 and 4. This corresponds to 100 μM Fe in equilibrium with mackinawite (Experiments 3-1, 3-5, 3-6, Panel A), 50 μM Fe + 50 μM S (Experiment 3-2, Panel B), and 50 mM Fe + 5 mM S (Experiment 4, Panel C). Speciation calculations done with Geochemist's Workbench v. 6.0 using a modified minteq database, and additional data on FeS_{aq} and mackinawite added from Rickard et al. (2006) and Benning et al. (2000), respectively.

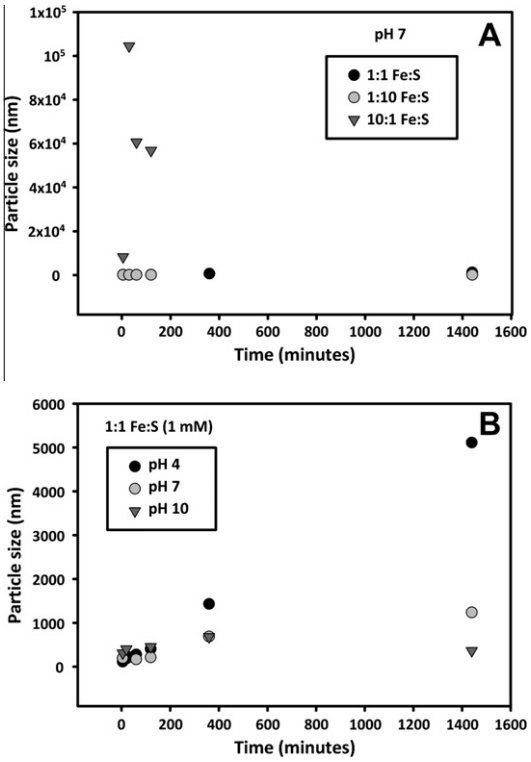

Fig. 3. Results of particle size experiments investigating the role of pH (6–8) and Fe:S ratio (1:10, 1:1, 10:1) on the kinetics of mackinawite aggregation.

isotope fractionation factors between aqueous Fe and mackinawite may be estimated by extrapolating the changes in δ^{56}Fe values over various extents of partial exchange, as calculated from the $\delta^{57/56}$Fe values, to 100% exchange. We note that plotting the data relative to the fraction exchanged, rather than a $^{56}Fe/^{54}Fe$–$^{57}Fe/^{54}Fe$ plot, as would typically be used with the three isotope method, small differences in bulk isotopic compositions of the various reactors may be accommodated; small differences in mass balances in the individual reactors would add scatter to a $^{56}Fe/^{54}Fe$–$^{57}Fe/^{54}Fe$ plot, decreasing the accuracy of extrapolating to 100% exchange. As noted in Section 2.3, we obtained good agreement between F calculated using aqueous or solid phases, which provides an internal check on the robustness of mass balance, confirming the confidence with which F may be used in extrapolating to 100% exchange.

Estimates for the equilibrium Fe isotope fractionation factors for experiments that only contained Fe^{2+}_{aq} (no added sulfide) are illustrated in Fig. 4. In all of the experiments shown in Fig. 4, >99.6% of the aqueous Fe existed as $Fe(H_2O)^{2+}_6$ based on thermodynamic calculations using Geochemists' Workbench, which is consistent with observed iron and sulfur speciation by voltammetry in these experiments. The weighted average fractionation determined in Experiments 3-1a and 3-1b, which did not involve dialysis membranes, produced a $\Delta^{56}Fe_{Fe(II)\text{-}mackinawite}$ fractionation of -0.21 ± 0.18‰; the weighted average of all four experiments (3-1a, 3-1b, 3-1c, and 3-1d) produced $\Delta^{56}Fe_{Fe(II)\text{-}mackinawite}$ fractionation of -0.32 ± 0.29‰ (Table 2). This fractionation is the same, within error at pH 7 and 35 °C (Experiment 3-3; $\Delta^{56}Fe_{Fe(II)\text{-}mackinawite} = -0.43 \pm 0.26$‰), pH 8 and 20 °C (Experiment 3-5; $\Delta^{56}Fe_{Fe(II)\text{-}mackinawite} = -0.32 \pm 0.09$‰), and pH 6 and 20 °C (Experiment 3-6; $\Delta^{56}Fe_{Fe(II)\text{-}mackinawite} = -0.36 \pm 0.07$‰). These results suggest that where aqueous Fe is dominated by $Fe(H_2O)^{2+}_6$, there is little effect of temperature and pH on the isotopic fractionation over the range explored in the current study.

In contrast, when free sulfide was added, the $\Delta^{56}Fe_{Fe(II)\text{–}mackinawite}$ fractionation increased in magnitude (Fig. 5). At pH 7 and 20 °C (Experiment 3-2), $\Delta^{56}Fe_{Fe(II)\text{–}mackinawite} = -0.64 \pm 0.36$‰, and at pH 7 and 35 °C (Experiment 3-4), $\Delta^{56}Fe_{Fe(II)\text{–}mackinawite} = -0.67 \pm 0.23$‰. Theses results suggest a measureable isotopic effect from added sulfide, but minimal temperature dependence over the range studied. The speciation changes upon addition of sulfide include a decrease in $Fe(H_2O)^{2+}_6$ and increase in $FeHS^+$ (from 0.09% to 63.2%), as well as an increase in FeS_{aq} (from 0.01% to 8.52%), based on thermodynamic calculations using Geochemists' Workbench, and this is consistent with observed iron and sulfur speciation by voltammetry in these experiments.

3.4. Temporal changes of apparent fractionation factors in FeS synthesis experiments influenced by particulate size

Synthesis experiments that were performed using Na_2S addition and isotopically "normal" Fe^{2+} (Experiment set 4, Table 1) show that the δ^{56}Fe values of aqueous Fe decreased with time and the δ^{56}Fe of the precipitated mackinawite increased with time under various pH conditions and initial Fe:S molar ratios (Supplementary Figure S2, Table S3). Such effects were initially observed by Butler et al. (2005). In order to test whether 0.22 μm filters were sufficient to separate mackinawite from the aqueous phase, the remaining supernatant was further filtered through a 0.025 μm filter paper. The results showed almost identical δ^{56}Fe values within analytical errors for aqueous and solid phases (see Experiment 4-1b F2 in Table S3), demonstrating that a 0.22 μm filter is sufficient to separate mackinawite and aqueous components in our experiments due to the tendency for mackinawite to aggregate. Efficient separation of mackinawite at these conditions is also consistent with our experiments showing particulate sizes increasing most rapidly at both lower pH and higher Fe:S ratio (Fig. 3). As we discuss below, these temporal changes in the synthesis experiments are interpreted to reflect isotopic re-equilibration after an initial kinetic isotope fractionation that was produced during precipitation.

4. DISCUSSION

4.1. Comparison with previous experiments

We infer the equilibrium fractionation factors via extrapolation to 100% exchange, a standard approach used with the three-isotope method. As we have noted in our previous work on Fe isotope fractionation factors using

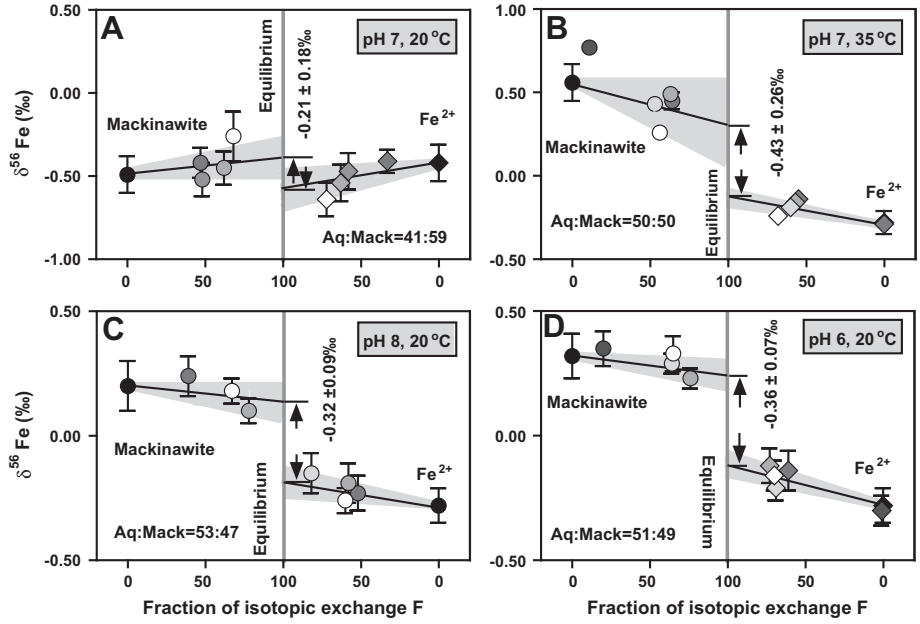

Fig. 4. Plot of δ^{56}Fe values versus percent of isotopic exchange for the isotope exchange experiments that initially contained only Fe^{2+}_{aq} (no initial sulfide). Equilibrium isotope compositions are inferred at 100% exchange. Symbols are shaded with darkest representing starting materials and lightest representing last time points. Symbol error bars are 1σ based on either measured errors or propagated errors. Errors in the inferred fractionation factor at 100% exchange are 2σ. Extrapolations were done by forcing the linear regression line to pass through the isotopic compositions of the starting materials. (A) Experiment at pH 7 and 20 °C (3-1), average for two duplicate experiments (3-1a and 3-1b). (B) Experiment at pH 7, 35 °C (Experiment 3-3). (C) Experiment at pH 8, 20 °C (Experiment 3-5). (D) Experiment at pH 6, 20 °C (Experiment 3-6).

Table 2
Extrapolated Fe isotope composition of aqueous Fe^{2+} and mackinawite at equilibrium.

Experiment[a]	Starting materials Outside membrane	Temp (°C)	pH	Aqueous δ^{56}Fe (‰)	error (‰)	Mackinawite δ^{56}Fe (‰)	error (‰)	$\Delta^{56}Fe_{Fe(II)-Mack}$ (‰)	2σ (‰)
3-1a	"normal" Fe^{2+}+"spiked" mackinawite	20	7	−0.60	0.04	−0.38	0.04	−0.22	0.11
3-1b	"normal" Fe^{2+}+"spiked" mackinawite	20	7	−0.60	0.07	−0.33	0.11	−0.28	0.25
3-1c	"spiked" Fe^{2+}+"normal" mackinawite	20	7	−0.57	0.08	0.02	0.02	−0.59	0.16
3-1d	"spiked" Fe^{2+}+"normal" mackinawite	20	7	−0.79	0.05	−0.63	0.20	−0.16	0.40
3-1	Weighted average	20	7	–	–	–	–	−0.32	0.29
3-2	"normal" Fe^{2+}+HS^-	20	7	−0.19	0.12	0.45	0.14	−0.64	0.36
3-3	"normal" Fe^{2+}	35	7	−0.11	0.03	0.32	0.13	−0.43	0.26
3-4	"normal" Fe^{2+}+HS^-	35	7	−0.10	0.11	0.56	0.04	−0.67	0.23
3-5	"normal" Fe^{2+}	20	8	−0.19	0.03	0.13	0.04	−0.32	0.09
3-6	"normal" Fe^{2+}	20	6	−0.12	0.03	0.24	0.03	−0.36	0.07

[a] Experiments 3-1 series were carried out without dialysis membrane. About equal concentrations of aqueous Fe^{2+} and mackinawite were mixed together and sampling was done by filtering suspension using 0.22 μm filter paper to separate mackinawite from aqueous Fe^{2+}.

the three-isotope method (e. g., Beard et al., 2010; Li et al., 2011; Wu et al., 2011, 2012), 100% exchange may not reflect true isotopic equilibrium, but if the exchange mechanism approaches equilibrium conditions, 100% exchange likely reflects the equilibrium fractionation factor. Our results for both equilibrium exchange experiments and FeS precipitation experiments are broadly consistent with those determined in previous studies, although some important distinctions exist. The equilibrium $^{56}Fe/^{54}Fe$ fractionation factor between $Fe(H_2O)^{2+}_6$ and mackinawite of -0.36 ± 0.07‰ at pH 6 and 20 °C (Fig. 4D) is close to that of -0.33 ± 0.12‰ determined at pH 4 and 25 °C by Guilbaud et al. (2011b), and this lies within error of the results we obtained at 20 °C for both pH 7 (Fig. 4A) and 8 (Fig. 4C). Guilbaud et al. (2011b) also employed a three-isotope method to determine equilibrium fractionation factors between Fe^{2+}_{aq} and mackinawite. Guilbaud et al. (2011b) speculated that their fractionation factors obtained at pH 4 would apply to neutral to alkaline pH, and our results confirm this prediction. The similarity in equilibrium fractionation factors determined with and without dialysis membranes suggests that these methods are comparable to each other, and the likely explanation is that rapid coarsening of mackinawite particulates allows sufficient

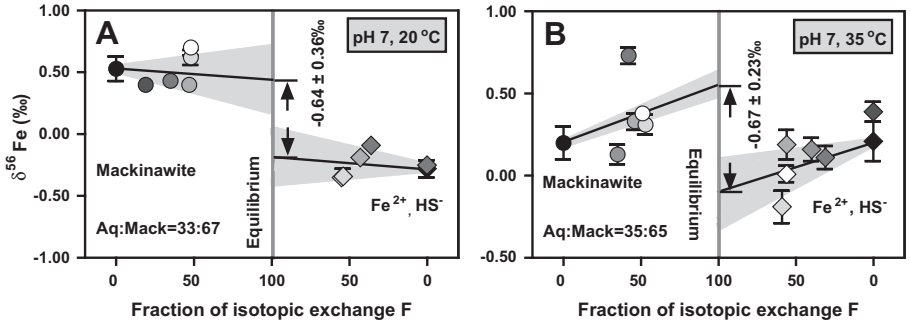

Fig. 5. Plot of δ^{56}Fe values versus percent of isotopic exchange for the isotope exchange experiments that initially contained both Fe^{2+}_{aq} and HS^- outside of the membrane (Experiments 3-2 (A) and 3-4 (B), Table 1). Equilibrium isotopic fractionations are inferred at 100% exchange, and errors noted are 2σ. Extrapolations were done by forcing the linear regression line to pass through the isotopic compositions of the starting materials. Symbols are shaded with darkest representing starting materials and lightest representing last time points. These experiments indicate an increase in the absolute values of the aqueous Fe-mackinawite fractionation when the proportion of aqueous Fe-S species is increased (compare with Fig. 4).

separation of aqueous phase from the solid phase by conventional filtration methods.

In contrast, however, the current study highlights a more important role in aqueous Fe–S speciation in the equilibrium Fe isotope fractionation factor than recognized in previous studies. Our results show that increases in the proportion of $FeHS^+$ and FeS_{aq} relative to $Fe(H_2O)_6^{2+}$ decreases the equilibrium aqueous Fe-mackinawite $^{56}Fe/^{54}Fe$ fractionation factor at room temperature by ~0.3‰. This in turn suggests that the equilibrium fractionation factor between $FeHS^+$ (and/or FeS_{aq}) and mackinawite is more negative that that between $Fe(H_2O)_6^{2+}$ and mackinawite.

Between 20 and 35 °C, there is little change in the aqueous Fe–mackinawite fractionation factor. For the non-sulfide bearing experiments, the $\Delta^{56}Fe_{Fe(II)-mackinawite}$ fractionation remains essentially unchanged at -0.43 ± 0.26‰ when temperature changed from 20 °C to 35 °C. In addition, the fractionation factor between aqueous Fe and mackinawite in the presence of HS^- does not change (-0.67 ± 0.23‰) with increasing temperature (Fig. 5). Small, but significant changes in the equilibrium aqueous Fe-mackinawite fractionations were noted by Guilbaud et al. (2011b), who measured a $\Delta^{56}Fe_{Fe(II)-mackinawite}$ fractionation of -0.52 ± 0.16‰ at 2 °C and -0.33 ± 0.12‰ at 25 °C, where $Fe(H_2O)_6^{2+}$ was the dominant aqueous species. Overall, the aqueous Fe-mackinawite fractionation is relatively insensitive to temperature, which in part simply reflects the small magnitude of these fractionation factors at low temperature.

Turning to the mackinawite synthesis experiments, in Fig. 6 we compare the results obtained in the current study to those of Butler et al. (2005) and Guilbaud et al. (2010), which were obtained at pH 4. Butler et al. (2005) interpreted their FeS precipitation experiments to record kinetic effects. They investigated the effects of aging the solution at 20 °C, and over time, the aqueous Fe-mackinawite fractionation decreased (Fig. 6), reflecting isotopic exchange between fluid and mineral. Guilbaud et al. (2010) extended the experiments to ~30 days, and their last time point produced a positive $\Delta^{56}Fe_{Fe(II)-mackinawite}$ fractionation factor. Based on the equilibrium $\Delta^{56}Fe_{Fe(II)-mackinawite}$ fractionation factor determined in the current study and by Guilbaud et al. (2011b), it is clear that the last time points in the FeS precipitation experiments of Butler et al. (2005) and Guilbaud et al. (2010) were far from equilibrium. Guilbaud et al. (2010) investigated nanoparticle size changes as related to their experiments, and together with the work of Wolthers et al. (2003), showed nanoparticle ripening was fairly limited and not different between pH 4 and 7. Ohfuji and Rickard (2006) have noted mackinawite aggregation is rapid and significant. We have combined these observations and showed that coarsening (including both ripening and aggregation) is dependent on pH and Fe:S ratio – if nanoparticles are not ripening significantly, the observation of micron-scale particulates must therefore reflect aggregates of nanoparticles, similar to what has been shown by Moreau et al. (2004) and Gilbert et al. (2003) for ZnS particles. Gilbert et al. (2003) additionally note that aggregation can affect transport of potential adsorbates within aggregates. Rapid particle aggregation of mackinawite nanoparticles may therefore result in an aggregate of nanoparticles containing an inner core of nanoparticles isolated from isotopic exchange with the bulk fluid. In summary, we interpret the results of Butler et al. (2005) and Guilbaud et al., 2010 to reflect the high degree of aggregation that mackinawite undergoes at low pH or high Fe:S ratios, which in turn limits its isotopic equilibration. In contrast, the FeS precipitation experiments obtained in the current study that were run at neutral pH reached the equilibrium aqueous Fe-mackinawite fractionation factor after 38 days (Fig. 6), indicating more extensive isotopic equilibration following precipitation. This directly reflects the lower rate of aggregation (Fig. 3) by mackinawite at neutral pH, as discussed above. These results suggest that mackinawite that formed in natural environments at near-neutral pH is unlikely to retain kinetic isotope fractionations, contrary to the arguments of Guilbaud et al. (2011a, 2011b), but is more likely to reflect equilibrium isotope compositions. Moreover, the results of our precipitation experiments confirm our inference that the equilibrium Fe^{2+}_{aq}-mackinawite fractionation is slightly negative. Collectively, these observations indicate that the Fe isotope compositions of mackinawite in natural

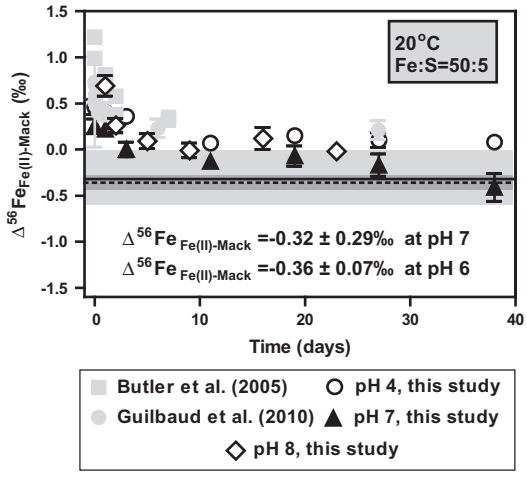

Fig. 6. Temporal variation in the $\Delta^{56}Fe_{Fe(II)aq-Mack}$ fractionation produced during precipitation of mackinawite. Experiments by Butler et al. (2005) and Guilbaud et al. (2010) used a Fe:S molar ratio of 50 mM:5 mM, and the pH was allowed to float to a final pH of 4 at 25 °C. Our experiment at pH 4 was a replicate of Butler et al. (2005)'s experiments but extended to longer times and it shows consistent results with those of Butler et al. and Guilbaud et al. (2010). The solid and dashed line indicates the equilibrium fractionation factor of $-0.32 \pm 0.29‰$ and $-0.36 \pm 0.07‰$ between aqueous Fe and mackinawite determined in this study at pH 7 and pH 6, respectively. Importantly, the mackinawite precipitation experiments done at pH 7 (this study) reached isotopic equilibrium for the final time point, in contrast to precipitation at pH 4 (Butler et al., 2005; Guilbaud et al., 2010), reflecting the greater extent of isotopic exchange at neutral pH.

systems may be different than those inferred from previous, low-pH experiments.

4.2. Comparison of fractionations predicted from theory and measured in experiment

Equilibrium isotope fractionation factors can be obtained through calculation of the reduced partition function ratio, or "beta factor" ($\beta^{56/54}$) for Fe species or minerals using *ab initio* or spectroscopic approaches. Under conditions of equilibrium, beta factors may be combined, as with any pathway-independent thermodynamic property. Using a variety of $\beta^{56/54}$ values for $Fe(H_2O)_6^{2+}$ and mackinawite, the predicted $\Delta^{56}Fe_{Fe(II)-mackinawite}$ fractionation at 20 °C ranges from +2.79‰ using the $\beta^{56/54}$ values for $Fe(H_2O)_6^{2+}$ and mackinawite from Rustad et al. (2010) and Polyakov and Soultanov (2011), respectively. If the uncertainty in the $\beta^{56/54}$ value for mackinawite is considered, the predicted $\Delta^{56}Fe_{Fe(II)-mackinawite}$ fractionation at 20 °C could be as low at +1.43‰. In contrast, a much larger fractionation factor is predicted if the $\beta^{56/54}$ value based on a DFT–PCM model for $Fe(H_2O)_6^{2+}$ is used from Anbar et al. (2005); in this case, the predicted $\Delta^{56}Fe_{Fe(II)-mackinawite}$ fractionation at 20 °C is +4.89‰. These predicted equilibrium fractionation factors are strongly inconsistent with the experimental results of the current study or those obtained by Guilbaud et al. (2011b).

Discrepancies between predicted and experimentally determined equilibrium Fe isotope fractionation factors have been recently discussed in the literature (Beard et al., 2010; Rustad et al., 2010; Polyakov and Soultanov, 2011), and the consensus for systems that do not involve sulfide is that previously calculated $\beta^{56/54}$ values for aqueous Fe species have generally been too high because the effects of extended hydration spheres were not included. Clearly, however, the experimental results obtained here and by Guilbaud et al. (2011b) again raise the issue of disagreement between predicted and measured equilibrium Fe isotope fractionation factors, at least in the case of sulfide-bearing systems. For comparison, the predicted fractionation between $Fe(H_2O)_6^{2+}$ and another FeS mineral, troilite, range from +1.41 to +3.51‰, calculated from the range in $\beta^{56/54}$ factors that have been proposed for $Fe(H_2O)_6^{2+}$ (Schauble et al., 2001; Anbar et al., 2005; Domagal-Goldman and Kubicki 2008; Ottonello and Zuccolini 2009; Rustad et al., 2010), and using the $\beta^{56/54}$ factor for troilite published by Polyakov et al. (2007). Considering that the structure of troilite and mackinawite is dramatically different, where Fe is octahedrally coordinated by S in troilite, but tetrahedrally coordinated in mackinawite, the difference between the predicted fractionations for two minerals is surprisingly small, implying that one of the calculated $\beta^{56/54}$ factors for Fe–S minerals may be wrong. We suggest that given the evidence that the $\beta^{56/54}$ factor for $Fe(H_2O)_6^{2+}$ published by Rustad et al. (2010) is correct (see discussion in Beard et al., 2010), the $\beta^{56/54}$ for mackinawite proposed by Polyakov and Soultanov (2011) may be significantly more in error than estimated. Polyakov and Soultanov (2011) acknowledge that their calculated $\beta^{56/54}$ value for mackinawite is based on very old spectroscopic data (Bertaut et al., 1965), which may have had significantly greater uncertainties than reported. Refinement of the $\beta^{56/54}$ factor for mackinawite is therefore important for future work.

4.3. Comparison of natural environments and experimental studies

Our experimental results, as well as those of Butler et al. (2005) and Guilbaud et al. (2010, 2011a, 2011b), provide an interpretive context for the large range in $\delta^{56}Fe$ values measured for pyrite in modern marine sediments (Severmann et al., 2006) and Precambrian rocks (Rouxel et al., 2005; Yamaguchi et al., 2005; Archer and Vance 2006). It has been suggested that two pathways may be important in pyrite formation in natural systems, the polysulfide and H_2S pathways. Both pathways involve precursor FeS phases, which appear to be essential in low temperature (<100 °C) environments (e.g., Morse et al., 1987; Rickard et al., 1995; Schoonen 2004). Understanding the origin of the Fe isotope compositions of pyrite from natural environments, therefore, requires tracing the isotopic compositions of aqueous Fe(II), FeS, and pyrite and their attendant fractionations.

We compare the Fe isotope compositions determined in modern marine sediments to those produced from various experimental studies in two parts, considering first the measured $\delta^{56}Fe$ values (Fig. 7), and second, the isotopic fractionations among various Fe components (Fig. 8). As previously discussed by Severmann et al. (2006) and

Johnson et al. (2008), pore fluid Fe(II) contents in modern marine sediments are highest where microbial dissimilatory iron reduction (DIR) is active, but low where high sulfide contents are generated by microbial dissimilatory sulfate reduction (DSR), and these relations produce distinct fields in terms of pore fluid Fe(II) contents and the fraction of pyritization (Fig. 7A). This in turn produces distinct fields for δ^{56}Fe values for pore fluid Fe(II) and the degree of pyritization for DIR and DSR (Fig. 7B), where DIR produces large quantities of aqueous Fe(II) that has low δ^{56}Fe values, and DSR produces small quantities of aqueous Fe(II) that has relatively high δ^{56}Fe values. Turning to the measured Fe isotope compositions for FeS and pyrite, FeS from the California margin sediments has moderately positive δ^{56}Fe values (Fig. 7C) and pyrite has moderately negative δ^{56}Fe values (Fig. 7D). Compared to the experimental study of Guilbaud et al. (2011a), who cast their data in terms of the degree of pyritization, a significantly more extreme range in isotopic compositions was produced in their laboratory experiments.

In Fig. 8 the Fe isotope fractionations among aqueous Fe(II), FeS, and pyrite determined from the experimental studies of Butler et al. (2005), Guilbaud et al. (2010, 2011a, 2011b), and the current study, are compared with those measured in modern marine sediments from the California margin (Severmann et al., 2006). The near-zero $Fe(II)_{aq}$–FeS fractionation measured in the California margin sediments that are dominated by sulfide (highest fraction of pyritization) overlap with the equilibrium $Fe(II)_{aq}$–FeS fractionation factor determined in the current study and by Guilbaud et al. (2011b). There is no evidence in the California margin sediments for the large positive kinetic $Fe(II)_{aq}$–FeS isotope fractionation during rapid precipitation of FeS, determined by Butler et al. (2005), Guilbaud et al. (2010), or in the current study. The very negative $Fe(II)_{aq}$–FeS fractionations measured in the California margin sediments are restricted to samples that have a low degree of pyritization, where Fe cycling is dominated by DIR (Fig. 8A). Where DIR is actively pumping low-δ^{56}Fe $Fe(II)_{aq}$, the highly negative $Fe(II)_{aq}$–FeS fractionations indicate that $Fe(II)_{aq}$ and FeS are not in isotopic equilibrium (Fig. 7A), although the slight trend in δ^{56}Fe values for FeS and the degree of pyritization in Fig. 7C is suggestive of some partial re-equilibration. The degree to which $Fe(II)_{aq}$ and FeS may be out of isotopic equilibrium in the DIR-dominated parts of the sediment column likely reflects the relative rate of production of low-δ^{56}Fe $Fe(II)_{aq}$ and the rate of isotopic exchange between $Fe(II)_{aq}$ and FeS. This contrasts with sediment sections that are rich in sulfide, where $Fe(II)_{aq}$ and FeS are close to isotopic equilibrium. It therefore appears that in the absence of extensive production of $Fe(II)_{aq}$ by DIR, Fe isotope equilibrium between $Fe(II)_{aq}$ and FeS is likely in natural systems.

Measured FeS–pyrite fractionations in the California margin sediments lie between +1 and +1.5‰ for samples whose Fe cycle is dominated by sulfide (high fraction of pyritization), and these generally decrease to ~+0.5‰ for samples where Fe cycling is dominated by DIR (Fig. 8B). These relations are interpreted to reflect partial Fe isotope re-equilibration of FeS and $Fe(II)_{aq}$ in the DIR-dominated

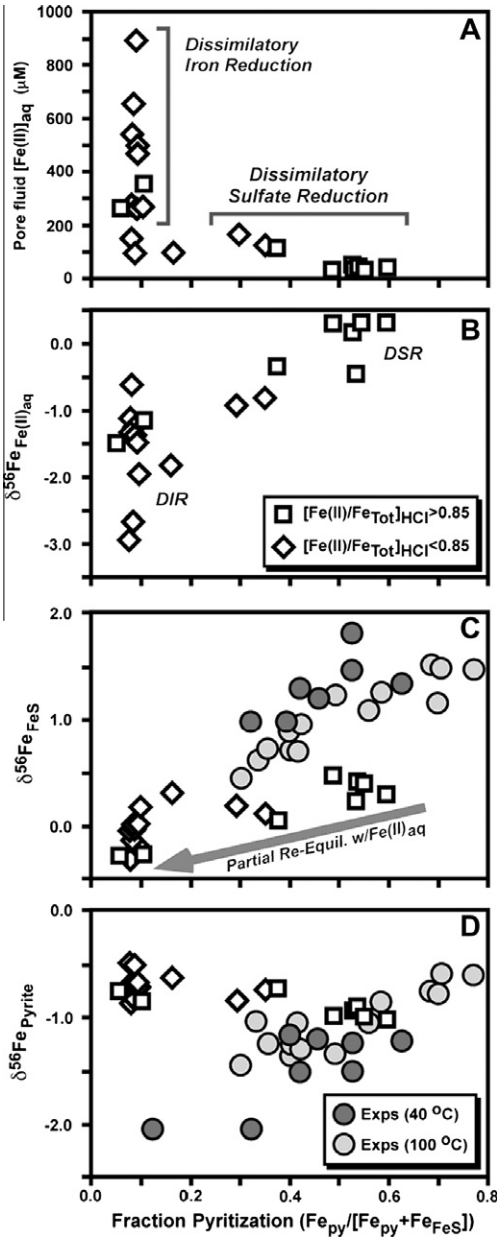

Fig. 7. Iron isotope compositions of aqueous Fe(II), FeS, and pyrite from the California continental margin (Severmann et al., 2006), and data produced from FeS and pyrite synthesis experiments at 40 and 100 °C by Guilbaud et al. (2011a); δ^{56}Fe values from Guilbaud et al. normalized to a starting composition of $\delta^{56}Fe = 0$. Data from the California margin reflect sediment sections where Fe cycling is dominated by microbial dissimilatory iron reduction (DIR), as well as those that are rich in sulfide, produced by microbial dissimilatory sulfate reduction (DSR). Solid-phase, HCl-extractable Fe is divided into samples that contain >85% Fe(II) of total Fe, and those that contain <85% Fe(II); as discussed in Johnson et al. (2008), δ^{56}Fe values calculated for FeS (part C) have the greatest confidence for samples that contain >85% Fe(II). Isotopic data for $Fe(II)_{aq}$ and pyrite from the California margin are as measured. All results, including the experimental study of Guilbaud et al. (2011a), cast in terms of fraction of pyritization.

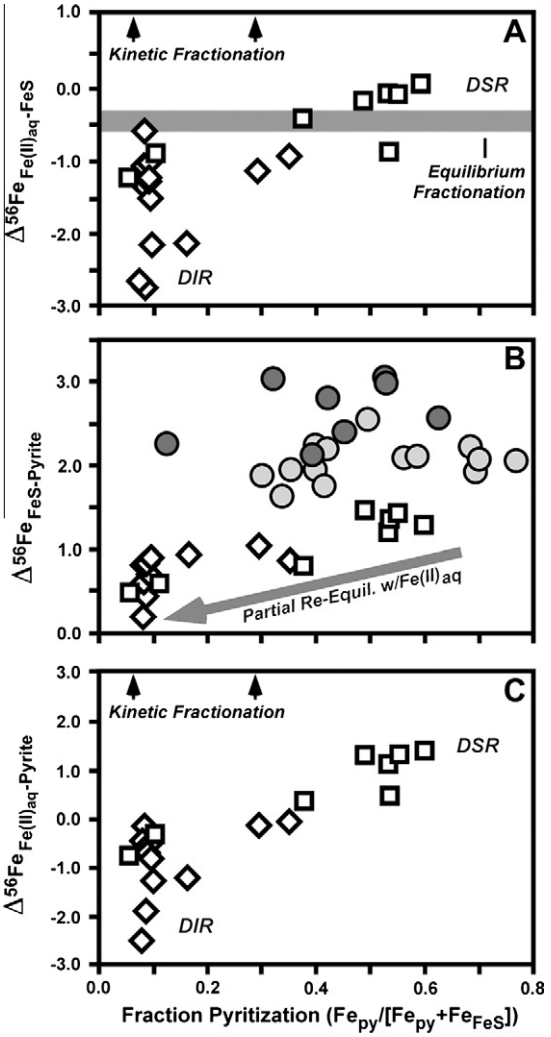

Fig. 8. Isotopic fractionations among $Fe(II)_{aq}$, FeS, and pyrite for modern marine sediments from the California continental margin (Severmann et al., 2006), the current study, and the experiments of Guilbaud et al. (2011a). The equilibrium $Fe(II)_{aq}$–FeS fractionation (grey bar in part A) encompasses those where aqueous Fe is $Fe(H_2O)_6^{2+}$ and for where sulfide was present (current study; Guilbaud et al., 2011b). Arrows note direction of kinetic isotope fractionation produced during rapid precipitation of FeS from $Fe(II)_{aq}$ (part A; Butler et al., 2005; Guilbaud et al., 2010), as well as rapid conversion of FeS to pyrite (part C; Guilbaud et al., 2011a). All results cast in terms of degree of pyritization, as in Fig. 7.

sediment sections, as discussed above. Much more extreme FeS–pyrite isotope fractionations were measured in the experimental study of Guilbaud et al. (2011a), who studied conversion of FeS to pyrite at 40 and 100 °C over periods of hours to days. Guilbaud et al. (2011a) argued that such large FeS–pyrite fractionations could be an explanation for negative δ^{56}Fe values measured for pyrite in the rock record, if such pyrite was produced by small extents of pyritization, where the greatest lowering of δ^{56}Fe values occurs in their experiments (Fig. 7D). There have been no experimental determinations of the Fe isotope fractionation between pyrite and other Fe species under demonstrably equilibrium conditions, but the very high $\beta^{56/54}$ factor for pyrite that is calculated by different methods, including *ab initio* (Blanchard et al., 2009) and Mössbauer (Polyakov et al., 2007) approaches suggests that, under equilibrium conditions, pyrite should have one of the highest δ^{56}Fe values of any mineral. The positive FeS–pyrite fractionations measured either in the California margin sediments or in the experiments of Guilbaud et al. (2011a), therefore, likely reflect non-equilibrium fractionations, consistent with expectations based on pyrite formation pathways (e.g., Butler et al., 2005).

Finally, the measured $Fe(II)_{aq}$–pyrite fractionations from the California margin sediments are compared to the fraction of pyritization in Fig. 8C. Based on the relations among the different Fe pools and isotopic compositions discussed above, it is not anticipated that the $Fe(II)_{aq}$–pyrite fractionations in the California margin sediments should reflect equilibrium conditions. The highly negative $Fe(II)_{aq}$–pyrite fractionations measured for samples that are dominated by DIR (low fraction of pyritization) simply reflects the very low-δ^{56}Fe values produced for $Fe(II)_{aq}$ by DIR, as discussed above. In contrast, the positive $Fe(II)_{aq}$–pyrite fractionations that are associated with samples dominated by DSR are in the same direction as the kinetic fractionation model proposed by Guilbaud et al. (2011a), although they do not reach the extreme values of the Guilbaud et al. (2011a) model.

4.4. Implications for Fe isotope compositions of pyrite in the rock record

Guilbaud et al. (2011a) suggested that the entire range in δ^{56}Fe values for pyrite in the rock record may be explained by a two-step process of kinetic isotope fractionations, first involving precipitation of FeS from $Fe(II)_{aq}$, and second, conversion of FeS to pyrite. Guilbaud et al. argue that the range in δ^{56}Fe values for pyrite requires neither redox changes nor microbial Fe cycling. To produce the negative δ^{56}Fe values for pyrite that are common in Neoarchean and Paleoproterozoic marine sedimentary rocks (e.g., Rouxel et al., 2005; Yamaguchi et al., 2005), Guilbaud et al. (2011a) invoke the maximum kinetic isotope fractionation observed in experiments between $Fe(II)_{aq}$ and FeS, and restrict the proportion of conversion of $Fe(II)_{aq}$ to FeS to relatively small proportions of the initial $Fe(II)_{aq}$ pool, followed by a kinetic isotope fractionation upon conversion of FeS to pyrite. The applicability of these results to the ancient rock record has been debated in Czaja et al. (2012) and Guilbaud et al. (2012).

Based on the experimental results obtained in the current study, the conditions favored by Guilbaud et al. (2011a) seem unlikely, given the fact that under neutral pH conditions (as studied here) the initially large kinetic $Fe(II)_{aq}$–FeS fractionation produced during FeS precipitation was largely erased by isotopic re-equilibration over several weeks (Fig. 6). Our results show that the conditions of particle aggregation seem to play a critical role in the preservation of the kinetic isotope fractionation levels where low pH and high Fe:S ratios trend towards more rapid aggregation and associated FeS core material that would

be isolated from equilibrium processes. The results obtained in the current study at neutral pH are important in this regard, in contrast to those obtained at low pH in prior studies, because pore fluids in modern anoxic marine sediments are characterized by near neutral pH (~6.5) to slightly alkaline pH values (~ 8) (e.g., Bischoff and Sayles 1972; Froelich et al., 1979; Walter and Burton 1990; Morse et al., 1992). The pH values of the pore fluids in authigenic and early diagenetic environments in the Precambrian are not well constrained, given the fact that estimates for the pH of the Precambrian seawater vary greatly, ranging from 5.5 to 9 (Kempe and Degens 1985; Grotzinger and Kasting 1993; Ohmoto et al., 2004). It is important to note, however, that microbial diagenesis involving both sulfate and iron reduction produces alkalinity, and so we infer that pore fluids should have had neutral to alkaline pH. That the $Fe(II)_{aq}$–FeS fractionations measured for samples from the California margin that have high degrees of pyritization lie close to the equilibrium fractionation provides strong support for expecting isotopic equilibrium between Fe^{2+}_{aq} and FeS, rather than the extreme fractionation favored in the model of Guilbaud et al. (2011a).

5. CONCLUSIONS

Equilibrium Fe isotope fractionation factors among aqueous iron, aqueous FeS clusters (FeS_{aq}), and nanoparticulate mackinawite have been determined in this study using a three-isotope method. As indicated by voltammetry and geochemical modeling, the major species are $Fe^{2+}(H_2O)_6$ (99.6%) for the experiments with Fe^{2+}_{aq} and mackinawite, and change to $FeHS^+$ (63.2%)>$Fe(H_2O)^{2+}_6$ (28.2%)>FeS_{aq} (8.52%) for experiments with Fe^{2+}_{aq}, HS^-, and mackinawite at pH 7. The equilibrium $^{56}Fe/^{54}Fe$ fractionation factor at 20 °C and pH 7 has been determined to be -0.32 ± 0.29 $(2\sigma)‰$ between Fe^{2+}_{aq} and mackinawite. This fractionation factor remained essentially unchanged with varying pH (6–8) and temperature conditions (20–35 °C). When free sulfide was added to the system, however, the fractionation factor decreased ~0.3‰ as a result of increases in the proportion of $FeHS^+$ and FeS_{aq} relative to $Fe(H_2O)^{2+}_6$. Our replicate of Butler et al.'s and Guilbaud et al.'s precipitation experiments at pH 4, show broadly consistent results: over time, the aqueous Fe-mackinawite fractionation decreased and changed from a positive value to more negative values, moving towards the equilibrium fractionation factor. The apparent isotopic fractionation, however, was still far from equilibrium after 38 days at pH 4 conditions, reflecting the high rate of aggregation that mackinawite undergoes at low pH, which limits isotopic equilibration. In contrast, the FeS precipitation experiments obtained in the current study that were run at neutral pH reached the equilibrium aqueous Fe-mackinawite fractionation factor after 38 days, indicating more extensive isotopic equilibration following precipitation, reflecting a lower degree of particle aggregation at neutral pH. These results suggest that mackinawite that formed in natural environments at near-neutral pH are unlikely to retain kinetic isotope fractionations, but are more likely to reflect equilibrium isotope compositions. Although the pH of pore fluids in Precambrian diagenetic sediments is unknown, if either microbial sulfate or iron reduction occurred, the alkalinity that these processes produce suggests that such fluids would have neutral to alkaline pH. We conclude that the Guilbaud et al. (2011a) model, which has been debated (Czaja et al., 2012; Guilbaud et al., 2012), for Fe isotope fractionation of Fe sulfides likely represents extreme experimental conditions that may be rare in marine diagenetic systems.

ACKNOWLEDGEMENTS

This work was supported by National Science Foundation grant EAR-0635593 (Johnson and Beard), EAR-0635523 (Druschel), EAR 0955639 (Druschel), and ACS-PRF 43356-GB2 (Druschel). Druschel gratefully acknowledges the work of several students who assisted with different parts of the lab work at the University of Vermont, including Harry Oduro, Jessica Sperling, and Christine Cramer. We thank AE D. Vance and three anonymous reviewers for helpful comments on the manuscript.

APPENDIX A. SUPPLEMENTARY DATA

Supplementary data associated with this article can be found, in the online version, at http://dx.doi.org/10.1016/j.gca.2012.04.047.

REFERENCES

Anbar A. D., Jarzecki A. A. and Spiro T. G. (2005) Theoretical investigation of iron isotope fractionation between $Fe(H_2O)_6^{3+}$ and $Fe(H_2O)_6^{2+}$: implications for iron stable isotope geochemistry. *Geochim. Cosmochim. Acta* **69**, 825–837.

Archer C. and Vance D. (2006) Coupled Fe and S isotope evidence for Archean microbial Fe(III) and sulfate reduction. *Geology* **34**, 153–156.

Beard B. L., Handler R. M., Scherer M. M., Wu L., Czaja A. D., Heimann A. and Johnson C. M. (2010) Iron isotope fractionation between aqueous ferrous iron and goethite. *Earth Planet. Sci. Lett.* **295**, 241–250.

Beard B. L., Johnson C. M., Skulan J. L., Nealson K. H., Cox L. and Sun H. (2003) Application of Fe isotopes to tracing the geochemical and biological cycling of Fe. *Chem. Geol.* **195**, 87–117.

Benning L. G., Wilkin R. T. and Barnes H. L. (2000) Reaction pathways in the Fe–S system below 100 °C. *Chem. Geol.* **167**, 25–51.

Berner R. A. (1970) Sedimentary pyrite formation. *Am. J. Sci.* **268**, 1–23.

Bertaut E. F., Burlet P. and Chappart J. (1965) Sur l'absence d'ordre magnetique dans la forme quadratique de FeS. *Solid State Commun.* **3**, 335–338.

Bischoff J. L. and Sayles F. L. (1972) Pore fluid and mineralogical studies of recent marine sediments; Bauer Depression region of East Pacific Rise. *J. Sediment. Res.* **42**, 711–724.

Blanchard M., Poitrasson F., Méheut M., Lazzeri M., Mauri F. and Balan E. (2009) Iron isotope fractionation between pyrite (FeS_2), hematite (Fe_2O_3) and siderite ($FeCO_3$): a first-principles density functional theory study. *Geochim. Cosmochim. Acta* **73**, 6565–6578.

Butler A. (2005) Marine siderophores and microbial iron mobilization. *Biometals* **18**, 369–374.

Butler I. B., Archer C., Vance D., Oldroyd A. and Rickard D. (2005) Fe isotope fractionation on FeS formation in ambient aqueous solution. *Earth Planet. Sci. Lett.* **236**, 430–442.

Butler I. B. and Rickard D. (2000) Framboidal pyrite formation via the oxidation of iron (II) monosulfide by hydrogen sulphide. *Geochim. Cosmochim. Acta* **64**, 2665–2672.

Cotton F. A., Daniels L. M., Murillo C. A. and Quesada J. F. (1993) Hexaaqua dipositive ions of the first transition series: new and accurate structures; expected and unexpected trends. *Inorg. Chem.* **32**, 4861–4867.

Czaja A. D., Johnson C. M., Yamaguchi K. E. and Beard B. L. (2012) Comment on "Abiotic Pyrite Formation Produces a Large Fe Isotope Fractionation". *Science* **335**, 538.

Dauphas N., Cates N. L., Mojzsis S. J. and Busigny V. (2007) Identification of chemical sedimentary protoliths using iron isotopes in the >3750 Ma Nuvvuagittuq supracrustal belt, Canada. *Earth Planet. Sci. Lett.* **254**, 358–376.

Davison W., Phillips N. and Tabner B. J. (1999) Soluble iron sulfide species in natural waters: reappraisal of their stoichiometry and stability constants. *Aquat. Sci. Res. Across Boundaries* **61**, 23–43.

Domagal-Goldman S. D. and Kubicki J. D. (2008) Density functional theory predictions of equilibrium isotope fractionation of iron due to redox changes and organic complexation. *Geochim. Cosmochim. Acta* **72**, 5201–5216.

Druschel G. K., Emerson D., Sutka R., Suchecki P. and Luther Iii G. W. (2008) Low-oxygen and chemical kinetic constraints on the geochemical niche of neutrophilic iron(II) oxidizing microorganisms. *Geochim. Cosmochim. Acta* **72**, 3358–3370.

Druschel G.K., Sutka R., Emerson D., Luther G.W., Kraiya C. and Glazer B. (2004) Voltammetric investigation of Fe–Mn–S species in a microbially active wetland. In *Proceedings of the Eleventh International Symposium on Water-Rock Interaction WRI-11* (eds. R.B. Wanty and R.R. Seals). Taylor & Francis. pp. 1191–1194.

Froelich P. N., Klinkhammer G. P., Bender M. L., Luedtke N. A., Heath G. R., Cullen D., Dauphin P., Hammond D., Hartman B. and Maynard V. (1979) Early oxidation of organic matter in pelagic sediments of the eastern equatorial Atlantic: suboxic diagenesis. *Geochim. Cosmochim. Acta* **43**, 1075–1090.

Gilbert B., Zhang H., Huang F., Finnegan M. P., Waychunas G. A. and Banfield J. F. (2003) Spcial phase transformation and crystal growth pathways observed in nanoparticles. *Geochem. Trans.* **4**, 20–27.

Glazer B. T., Luther Iii G. W., Konovalov S. K., Friederich G. E., Trouwborst R. E. and Romanov A. S. (2006) Spatial and temporal variability of the Black Sea suboxic zone. *Deep Sea Res. Part II* **53**, 1756–1768.

Grotzinger J. P. and Kasting J. F. (1993) New constraints on Precambrian ocean composition. *J. Geol.* **101**, 235–243.

Guilbaud R., Butler I. B. and Ellam R. M. (2011a) Abiotic pyrite formation produces a large Fe isotope fractionation. *Science* **332**, 1548–1551.

Guilbaud R., Butler I. B., Ellam R. M. and Rickard D. (2010) Fe isotope exchange between Fe(II)aq and nanoparticulate mackinawite (FeSm) during nanoparticle growth. *Earth Planet. Sci. Lett.* **300**, 174–183.

Guilbaud R., Butler I. B., Ellam R. M., Rickard D. and Oldroyd A. (2011b) Experimental determination of the equilibrium Fe isotope fractionation between Fe^{2+aq} and FeS_m (mackinawite) at 25 and 2 °C. *Geochim. Cosmochim. Acta* **75**, 2721–2734.

Guilbaud R., Butler I. B. and Ellam R. M. (2012) Response to comment on "Abiotic Pyrite Formation Produces a Large Fe Isotope Fractionation". *Science* **335**, 538.

Hofmann A., Bekker A., Rouxel O., Rumble D. and Master S. (2009) Multiple sulphur and iron isotope composition of detrital pyrite in Archaean sedimentary rocks: a new tool for provenance analysis. *Earth Planet. Sci. Lett.* **286**, 436–445.

Johnson C. M., Beard B. L., Klein C., Beukes N. J. and Roden E. E. (2008) Iron isotopes constrain biologic and abiologic processes in banded iron formation genesis. *Geochim. Cosmochim. Acta* **72**, 151–169.

Kempe S. and Degens E. T. (1985) An early soda ocean? *Chem. Geol.* **53**, 95–108.

Labrenz M., Druschel G. K., Thomsen-Ebert T., Gilbert B., Welch S. A., Kemner K. M., Logan G. A., Summons R. E., De Stasio G. and Bond P. L., et al. (2000) Formation of sphalerite (ZnS) deposits in natural biofilms of sulfate-reducing bacteria. *Science* **290**, 1744–1747.

Li W., Beard B. L. and Johnson C. M. (2011) Exchange and fractionation of Mg isotopes between epsomite and saturated $MgSO_4$ solution. *Geochim. Cosmochim. Acta* **75**, 1814–1828.

Liu X. and Millero F. J. (2002) The solubility of iron in seawater. *Mar. Chem.* **77**, 43–54.

Luther G., Glazer B., Ma S., Trouwborst R., Shultz B., Druschel G. and Kraiya C. (2003) Iron and sulfur chemistry in a stratified lake: evidence for iron-rich sulfide complexes. *Aquat. Geochem.* **9**, 87–110.

Luther G. W. and Ferdelman T. G. (1993) Voltammetric characterization of iron(II) sulfide complexes in laboratory solutions and in marine waters and porewaters. *Environ. Sci. Technol.* **27**, 1154–1163.

Luther G. W. and Rickard D. (2005) Metal sulfide cluster complexes and the biogeochemical importance in the environment. *J. Nanopart. Res.* **7**, 389–407.

Luther G. W., Rickard D. T., Theberge S. and Olroyd A. (1996) Determination of metal (bi)sulfide stability constants of Mn^{2+}, Fe^{2+}, Co^{2+}, Ni^{2+}, Cu^{2+}, and Zn^{2+} by voltammetric methods. *Environ. Sci. Technol.* **30**, 671–679.

Luther G. W., Theberge S. M. and Rickard D. T. (1999) Evidence for aqueous clusters as intermediates during zinc sulfide formation. *Geochim. Cosmochim. Acta* **63**, 3159–3169.

Luther G. W., Theberge S. M., Rozan T. F., Rickard D., Rowlands C. C. and Oldroyd A. (2002) Aqueous copper sulfide clusters as intermediates during copper sulfide formation. *Environ. Sci. Technol.* **36**, 394–402.

Luther, III, G. W. (1991) Pyrite synthesis via polysulfide compounds. *Geochim. Cosmochim. Acta* **55**, 2839–2849.

Matsuhisa Y., Goldsmith J. R. and Clayton R. N. (1978) Mechanisms of hydrothermal crystallization of quartz at 250 °C and 15 kbar. *Geochim. Cosmochim. Acta* **42**, 173–182.

Moreau J. W., Webb R. I. and Banfield J. F. (2004) Ultrastructure, aggregation-state, and crystal growth of biogenic nanocrystalline sphalerite and wurtzite. *Am. Mineral.* **89**, 950–960.

Morse J. W., Cornwell J. C., Arakaki T., Lin S. and Huerta-Diaz M. (1992) Iron sulfide and carbonate mineral diagenesis in Baffin Bay, Texas. *J. Sediment. Petrol.* **62**, 671–680.

Morse J. W., Millero F. J., Cornwell J. C. and Rickard D. (1987) The chemistry of the hydrogen sulfide and iron sulfide systems in natural waters. *Earth Sci. Rev.* **24**, 1–42.

Nishizawa M., Yamamoto H., Ueno Y., Tsuruoka S., Shibuya T., Sawaki Y., Yamamoto S., Kon Y., Kitajima K. and Komiya T., et al. (2010) Grain-scale iron isotopic distribution of pyrite from Precambrian shallow marine carbonate revealed by a femtosecond laser ablation multicollector ICP-MS technique: possible proxy for the redox state of ancient seawater. *Geochim. Cosmochim. Acta* **74**, 2760–2778.

Ohfuji H. and Rickard D. (2006) High resolution transmission electron microscopic study of synthetic nanocrystalline mackinawite. *Earth Planet. Sci. Lett.* **241**, 227–233.

Ohmoto H., Watanabe Y. and Kumazawa K. (2004) Evidence from massive siderite beds for a CO_2-rich atmosphere before ~1.8 billion years ago. *Nature* **429**, 395–399.

Ottonello G. and Zuccolini M. V. (2009) Ab-initio structure, energy and stable Fe isotope equilibrium fractionation of some geochemically relevant H–O–Fe complexes. *Geochim. Cosmochim. Acta* **73**, 6447–6469.

Polyakov V. B., Clayton R. N., Horita J. and Mineev S. D. (2007) Equilibrium iron isotope fractionation factors of minerals: reevaluation from the data of nuclear inelastic resonant X-ray scattering and Mössbauer spectroscopy. *Geochim. Cosmochim. Acta* **71**, 3833–3846.

Polyakov V. B. and Soultanov D. M. (2011) New data on equilibrium iron isotope fractionation among sulfides: constraints on mechanisms of sulfide formation in hydrothermal and igneous systems. *Geochim. Cosmochim. Acta* **75**, 1957–1974.

Rickard D. (1975) Kinetics and mechanism of pyrite formation at low temperatures. *Am. J. Sci.* **275**, 636–652.

Rickard D. (1997) Kinetics of pyrite formation by the H_2S oxidation of iron (II) monosulfide in aqueous solutions between 25 and 125 °C: the rate equation. *Geochim. Cosmochim. Acta* **61**, 115–134.

Rickard D., Griffith A., Oldroyd A., Butler I. B., Lopez-Capel E., Manning D. A. C. and Apperley D. C. (2006) The composition of nanoparticulate mackinawite, tetragonal iron(II) monosulfide. *Chem. Geol.* **235**, 286–298.

Rickard D. and Luther, III, G. W. (1997) Kinetics of pyrite formation by the H_2S oxidation of iron (II) monosulfide in aqueous solutions between 25 and 125 °C: the mechanism. *Geochim. Cosmochim. Acta* **61**, 135–147.

Rickard D., Schoonen M. A. A. and Luther, III, G. W. (1995) Chemistry of iron sulfides in sedimentary environments. In *Geochemical Transformations of Sedimentary Sulfur* (eds. M. A. Vairavamurthy and M. A. A. Schoonens). American Chemical Society. pp. 168–193.

Rouxel O. J., Bekker A. and Edwards K. J. (2005) Iron isotope constraints on the Archean and Paleoproterozoic ocean redox state. *Science* **307**, 1088–1091.

Rouxel O. J., Bekker A. and Edwards K. J. (2006) Response to comment on "Iron isotope constrains on the archean and paleoproterozoic ocean redox state". *Science* **311**, 177b.

Rustad J. R., Casey W. H., Yin Q.-Z., Bylaska E. J., Felmy A. R., Bogatko S. A., Jackson V. E. and Dixon D. A. (2010) Isotopic fractionation of Mg^{2+}(aq), Ca^{2+}(aq), and Fe^{2+}(aq) with carbonate minerals. *Geochim. Cosmochim. Acta* **74**, 6301–6323.

Schauble E. A. (2004) Applying stable isotope fractionation theory to new systems. *Rev. Mineral. Geochem.* **55**, 65–111.

Schauble E. A., Rossman G. R. and Taylor H. P. (2001) Theoretical estimates of equilibrium Fe-isotope fractionations from vibrational spectroscopy. *Geochim. Cosmochim. Acta* **65**, 2487–2497.

Schoonen M. A. A. (2004) Mechanisms of sedimentary pyrite formation. *Geol. Soc. Amer. Spec. Pap.* **379**, 117–133.

Schoonen M. A. A. and Barnes H. L. (1991) Reactions forming pyrite and marcasite from solution: II. Via FeS precursors below 100 °C. *Geochim. Cosmochim. Acta* **55**, 1505–1514.

Severmann S., Johnson C. M., Beard B. L. and McManus J. (2006) The effect of early diagenesis on the Fe isotope compositions of porewaters and authigenic minerals in continental margin sediments. *Geochim. Cosmochim. Acta* **70**, 2006–2022.

Taylor P., Rummery T. E. and Owen D. G. (1979) Reactions of iron monosulfide solids with aqueous hydrogen sulfide up to 160 °C. *J. Inorg. Nucl. Chem.* **41**, 1683–1687.

Theberge S. M. and Luther G. W. (1997) Determination of the electrochemical properties of a soluble aqueous FeS species present in sulfidic solutions. *Aquat. Geochem.* **3**, 191–211.

Thompson R. A. and Helz G. R. (1994) Copper speciation in sulfidic solutions at low sulfur activity: further evidence for cluster complexes? *Geochim. Cosmochim. Acta* **58**, 2971–2983.

Walter L. M. and Burton E. A. (1990) Dissolution of Recent platform carbonate sediments in marine pore fluids. *Am. J. Sci.* **290**, 601–643.

Wei D. and Osseo-Asare K. (1996) Particulate pyrite formation by the Fe^{3+}/HS^- reaction in aqueous solutions: effects of solution composition. *Colloids Surf., A* **118**, 51–61.

Whitehouse M. J. and Fedo C. M. (2007) Microscale heterogeneity of Fe isotopes in >3.71 Ga banded iron formation from the Isua Greenstone Belt, southwest Greenland. *Geology* **35**, 719–722.

Wolthers M., Van der Gaast S. J. and Rickard D. (2003) The structure of disordered mackinawite. *Am. Mineral.* **88**, 2007–2015.

Wu L., Beard B. L., Roden E. E. and Johnson C. M. (2011) Stable iron isotope fractionation between aqueous Fe(II) and hydrous ferric oxide. *Environ. Sci. Technol.* **45**, 1847–1852.

Wu L., Percak-Dennett E., Beard B. L., Roden E. E. and Johnson C. M. (2012) Stable iron isotope fractionation between aqueous Fe(II) and model Archean ocean Fe–Si coprecipitates and implications for iron isotope variations in the ancient rock record. *Geochim. Cosmochim. Acta* **84**, 14–28.

Yamaguchi K. E., Johnson C. M., Beard B. L. and Ohmoto H. (2005) Biogeochemical cycling of iron in the Archean-Paleoproterozoic Earth: constraints from iron isotope variations in sedimentary rocks from the Kaapvaal and Pilbara Cratons. *Chem. Geol.* **218**, 135–169.

Yamaguchi K. E. and Ohmoto H. (2006) Comment on "Iron isotope constraints on the Archean and Paleoproterozoic ocean redox state", by Rouxel et al.. *Science* **311**, 177a.

Associate editor: Derek Vance